IOP PUBLISHING JOURNAL OF PHYSICS D: APPLIED PHYSICS

J. Phys. D: Appl. Phys. **42** (2009) 135206 (11pp) doi:10.1088/0022-3727/42/13/135206

Characterization of an N_2 flowing microwave post-discharge by OES spectroscopy and determination of absolute ground-state nitrogen atom densities by TALIF

Et Es-sebbar, Y Benilan, A Jolly and M-C Gazeau

LISA, Universités Paris 12 et Paris 7, UMR CNRS 7583 du CNRS, 61 avenue du Général de Gaulle, 94010 Créteil Cedex, France

E-mail: essebbar@lisa.univ-paris12.fr and benilan@lisa.univ-paris12.fr

Received 10 April 2009, in final form 13 April 2009
Published 17 June 2009
Online at stacks.iop.org/JPhysD/42/135206

Abstract

A flowing microwave post-discharge source sustained at 2.45 GHz in pure nitrogen has been investigated by optical emission spectroscopy (OES) and two-photon absorption laser-induced fluorescence (TALIF) spectroscopy. Variations of the optical emission along the post-discharge (near, pink and late afterglow) have been studied and the gas temperature has been determined. TALIF spectroscopy has been used in the late afterglow to determine the absolute ground-state nitrogen atomic densities using krypton as a reference gas. Measurements show that the microwave flowing post-discharge is an efficient source of N (^{4}S) atoms in late afterglow. In our experimental conditions, the maximum N (^{4}S) density is about 2.2×10^{15} cm^{-3} for a pressure of 22 Torr, at 300 K. The decay of N (^{4}S) density as a function of the time spent in the quartz tube has been modelled and a wall recombination probability γ of $(2.1 \pm 0.3) \times 10^{-4}$ is obtained.

(Some figures in this article are in colour only in the electronic version)

1. Introduction

Recently, numerous works have been undertaken in order to characterize flowing post-discharges sustained in pure nitrogen as well as in N_2/Ar mixtures and in N_2 with small amounts of O_2, H_2 and CH_4. Indeed, these afterglow discharges generate highly active species that can be used for a wide variety of applications, including surface nitriding [1, 2], surface cleaning and treatments [3, 4] as well as sterilization purposes [5–8]. In this context, the kinetics of active species such as N, O and H atoms and metastable molecules are important to understand. Besides, a great number of experimental studies using microwave flowing post-discharge have been developed recently in order to simulate atmospheric chemistry, in particular in the frame of Titan atmospheric studies [9–12]. Microwave flowing post-discharges have many advantages mainly related to (i) their generation in different gas mixtures, (ii) their formation far from microwave discharge source, through gas flow at low temperature (≈300 K) and (iii) their low costs of operation with simple instruments (surfatron and quartz tube coupled to a microwave generator) in various gas pressures, flow rates, residence times and microwave discharge powers. In addition, the dissociation of N_2 mainly by electrons within the microwave discharge is easier than its dissociation by extreme ultraviolet photons ($\lambda < 90$ nm) which implies windowless experiments.

Several *in situ* diagnostics can be implemented to investigate flowing N_2 microwave post-discharge. Optical

emission spectroscopy (OES) has proved to be a very powerful tool largely used to characterize the plasma gas temperature. Moreover, this technique allows the determination of relative populations of radiative species. However, it does not give direct information on some of the relevant plasma and post-discharge quantities, such as the absolute ground-state nitrogen density although this parameter is required to understand the chemistry of the plasma discharge. Usually, this quantity is obtained by titration in the post-discharge [5, 6]. However, this method has no spatial resolution and is difficult to achieve at high gas pressure (above 6 Torr) [6]. Calibration by the titration method is consequently inappropriate to determine ground state atomic nitrogen densities in all conditions. Two-photon absorption laser-induced fluorescence (TALIF) spectroscopy is an efficient alternative.

TALIF diagnostic has high selectivity and sensitivity. Detection limits of species in the range of 10^{11}–10^{12} cm^{-3} can be achieved [13, 14]. In fact, it is a well-established method to measure atomic concentrations (N, H, O) in different types of plasma at low pressure [15–17] and at atmospheric pressure [18–21]. It has also been used in flames [22, 23] and can provide temporal and three-dimensional spatial resolution [24] because the interaction volume of the laser beam with the particles can be well defined. The behaviour of the species present in the plasma can thus be characterized such as their velocity distributions and subsequently the gas kinetics [25, 26]. TALIF measurements give the relative atom nitrogen densities since the cross section of two-photon excitation is unknown and the solid angle, in which the induced fluorescence is detected, is difficult to determine. In order to achieve absolute results, the induced fluorescence yield was calibrated using noble gas [18, 27]. The latter must have a two-photon resonance spectrally close to the atomic specie to be quantified. Here we have used krypton which is well suited for the calibration of ground-state atomic nitrogen N ($2p^3\ ^4S_{3/2}$). To our knowledge, only one paper deals with *in situ* measurements of ground-state nitrogen atom density in flowing post-discharge produced by a 433 MHz microwave source [26]. Here, we report the investigation of flowing N_2 post-discharge sustained by a 2.45 GHz microwave discharge by OES and TALIF. OES has been used to determine the gas temperature and to characterize the axial structure of the post-discharge. TALIF diagnostics has been used to determine the absolute ground-state nitrogen atom densities in the afterglow. We used experimental conditions of gas pressure ranging from 1 to 45 Torr, nitrogen gas flow rate between 20 and 500 sccm and microwave discharge power from 30 to 160 W.

Section 2 introduces the basic principles of TALIF spectroscopy as well as TALIF calibration by noble gases. The arrangement of TALIF spectroscopy diagnostic and microwave post-discharge is detailed in section 3. The OES analysis of N_2 flowing post-discharge used to describe the axial structure of dominant N_2^+ ($B\,^2\Sigma_u,\ v' \rightarrow X\,^2\Sigma_g,\ v''$) and N_2 ($C\,^3\Pi_u \rightarrow B\,^3\Pi_g,\ \Delta v = -2,\ \Delta v = -3$) emissions along the post-discharge as well as the axial profile of rotational temperature is described in section 4. Results concerning measurements of absolute ground state atomic nitrogen densities in the afterglow by TALIF are presented and discussed in the same section, followed by concluding remarks in section 5.

2. TALIF spectroscopy and calibration procedure: theoretical approaches

The principle of TALIF measurements has been described in various papers or reviews [13, 24–27]. For a simplified three-level excitation scheme, a specific atom or molecule generally in its ground-state level $|1\rangle$ is excited by the absorption of two UV photons inducing a resonant transition between the fundamental and the first allowed excited electronic level $|2\rangle$. It is followed by fluorescence towards a lower state $|3\rangle$. Under high laser flux, absorption of a third photon can lead to ionization of the excited atom which induces a decrease in the fluorescence. Collisional quenching at higher pressure can also be responsible for a loss in the fluorescence signal. In the case of low photon fluxes, the ground-state atomic densities remain almost the same and the integrated fluorescence signal (S_X) for specie X can be expressed as [25–27]:

$$S_X = n_X \frac{\Omega}{4\pi} \eta_X T_X G^{(2)} \sigma_X^{(2)} \left(\frac{E_X}{h\nu_X}\right)^2 G_X a_X, \qquad (1)$$

where n_X is the ground-state density of X, $\Omega/4\pi$ is the solid angle of the detection, η_X is the detector's quantum efficiency at the fluorescence wavelength, T_X is the transmission of the interferential filter, $G^{(2)}$ is a photon statistic factor for the absorption of two photons, the value of which is equal to 2 [27], $\sigma_X^{(2)}$ is the two-photon excitation cross section, $(E_X/h\nu_X)^2$ is the number of photons per pulse which depends on the laser energy E_X and on the photon energy $h\nu_X$, G_X is the detector amplification factor, and $a_X = A_{2k}/(A_2 + Q)$ is the branching ratio of the observed fluorescence transition which depends on A_{2k}, the transition probability, $A_2 = \sum_{k<2} A_{2k}$, the total transition probability of the excited level of a radiative transition $2 \rightarrow k$ and $Q = \sum_q k(q)\, n(q)$, the quenching rate that depends on the density $n(q)$ of the collision partners and $k(q)$ their corresponding quenching rate coefficients.

Some experimental parameters like the solid angle of emission and the two-photon excitation cross section are generally unknown so that TALIF studies can only lead to relative values of the densities. The use of reference gas source at a known density is therefore necessary to calibrate the experimental setup. According to expression (1) and by dividing the intensity (S_X) of X by the intensity (S_R) of a reference gas R, it is possible to determine the absolute density of X [25–27]:

$$n_X = n_R \frac{S_X}{S_R} \frac{\sigma_R^{(2)}}{\sigma_X^{(2)}} \left(\frac{E_R \nu_X}{E_X \nu_R}\right)^2 \frac{\eta_R T_R}{\eta_X T_X} \frac{G_R}{G_X} \frac{a_R}{a_X}. \qquad (2)$$

In our case, we use krypton (R = Kr) as a reference gas for the calibration of nitrogen atoms (figure 1). Excitation of nitrogen and krypton atoms (transitions N ($2p^3\ ^4S_{3/2}$) to N ($3p\ ^4S_{3/2}$) and Kr ($4p^6\ ^1S_0$) to Kr ($5p'\ [3/2]_2$) is induced by the absorption of two UV photon at λ = 206.72 nm and 204.20 nm, respectively. Spontaneous emission to lower electronic levels N ($3s\ ^4P_{1/2,3/2,5/2}$) and Kr ($5s'\ [1/2]_1$) can then be observed in the range 742–745 nm and at 826.3 nm, respectively. The calibration has been performed with a gas mixture (2%Kr–98%N_2) at a total pressure of 269 Torr. Those

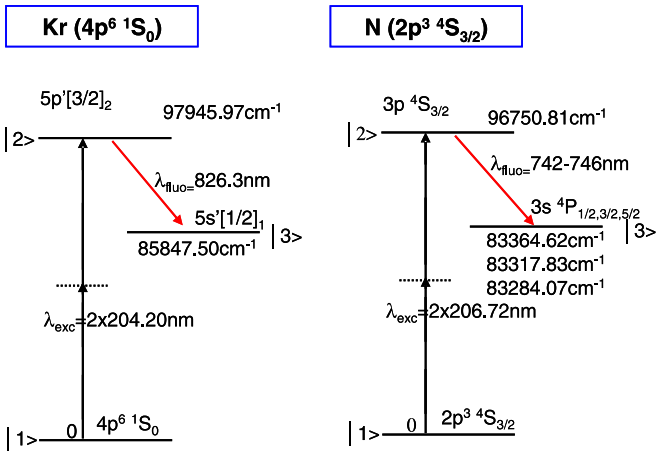

Figure 1. Energy level diagram and electronic transition for two-photon excitation laser-induced fluorescence of atomic nitrogen and krypton.

Table 1. Radiative lifetime and quenching coefficients of the excited state of nitrogen and krypton.

Excited state	τ (ns)	k_q (10^{-10} cm^3 s^{-1}) (N_2, Kr)	References
N (3s $^4P_{3/2}$)	29.6	0.41 3.16	[27]
Kr (5p′ [3/2]$_2$)	34.1	3.35 1.46	[27]

Table 2. Parameters involved in the N density calibration with krypton.

	Kr	N
ν(cm^{-1})	97 945.97	96 750.81
η (%)	7	9.8
T(%)	42.7	40.5

conditions correspond to a krypton density $n_{Kr} = 1.73 \times 10^{17}$ cm^{-3} at room temperature. For the ratio of the two-photon excitation cross sections, we use the value determined recently by Niemi *et al* [27], $\sigma^{(2)}_{Kr}/\sigma^{(2)}_{N} = 0.67$. The radiative lifetime of the excited state (τ) of nitrogen and krypton atoms and their quenching coefficients are given in table 1. The values of the other parameters involved in the determination of N (^{4}S) atom density through krypton calibration are presented in table 2.

3. Experimental details

3.1. Experimental setup of the TALIF Spectroscopy diagnostic

The experimental setup of the TALIF diagnostic is drawn schematically in figure 2(*a*). A pulsed Nd : YAG laser (Quanta-Ray Pro Series 230-30 by Spectra Physics) at 1064 nm with a pulse duration of 10 ns and a repetition rate of 10 Hz is coupled to a dye laser (Cobra-Stretch Dye Laser by Syrah) consisting of an oscillator formed by a grating resonator cavity and a preamplifier. The dye laser operates with a mixture of RhB/Rh101 in ethanol solution and is pumped by the second harmonic of the Nd : YAG laser at 532 nm. Tunable radiations in the range 598–636 nm with a maximum efficiency at 615 nm are generated. The laser energy typically reaches 150 mJ/pulse at 615 nm. At this wavelength, the laser resolution is 20 pm. The output frequency is doubled and then mixed with itself through respectively, a potassium dihydrogen phosphate (KDP) and a beta barium borate (BBO) crystal. After the KDP crystal, the polarization of the generated blue laser beam is rotated in order to coincide with the polarization of the fundamental red laser beam using a $\lambda/2$ wave plate. After the BBO crystal, a four mirrors system is used to separate the UV beam from the remaining blue and red radiations which are blocked. UV photons around 205 nm with a maximum energy of 5 mJ are obtained. By scanning the dye laser, UV radiation can be tuned to 206.72 nm and 204.20 nm to excite the nitrogen and krypton transition, respectively. Because two-photon excitation cross sections are low, the UV laser beam is focused at the centre of the post-discharge reactor chamber by a short focal lens ($f = 18$ cm): the density of photons passing through a 1 mm diameter diaphragm is then increased. The UV energy is monitored behind the reactor by a Joule-meter.

The fluorescence signal is measured perpendicularly to the incoming laser beam. A plano-convex lens (10 cm focal length, 5 cm diameter) images the detection volume onto the photomultiplier tube (R636-10 Hamamatsu). An interferential optical filter at 750 with 20 nm FWHM is used to select the induced fluorescence of N (3p $^4S_{3/2}$) $\rightarrow$ N (3s $^4P_{1/2,3/2,5/2}$) between 742 and 746 nm. Another filter at 830 nm with 20 nm FWHM allows to observe the 826.3 nm emission corresponding to Kr (5p′ [3/2]$_2$) $\rightarrow$ Kr (5 s′ [1/2]$_1$). The fluorescence signal is recorded through an oscilloscope (National Instrument). The acquisition system integrates the signal on a timescale of 100 ns since the relaxation processes have time constants of less than 80 ns. Scanning the dye laser close to the excitation wavelength of the nitrogen allows optimizing the recorded fluorescence intensity.

The experimental linewidth ($\Delta\nu_{exp}$) of the TALIF emission is equal to 0.6 cm^{-1}. At low gas pressure, it is the result of a convolution of a Doppler line profile ($\Delta\nu_D$) with the instrumental function of the laser ($\Delta\nu_L$). Assuming a Gaussian profile for the UV laser radiation, we have $\Delta\nu^2_{exp} = \Delta\nu^2_D + 2\Delta\nu^2_L$. Since the Doppler line width of the nitrogen transition at 96 750.81 cm^{-1} is $\Delta\nu_D = 0.32$ cm^{-1} at room temperature, the calculated laser line width $\Delta\nu_L$ is about 0.36 cm^{-1}.

3.2. Microwave discharge source and flowing post-discharge

The experimental apparatus of the microwave plasma and the flowing post-discharge is shown schematically in figure 2(*b*). The discharge is sustained by a 2.45 GHz surfatron (SAIREM) and surfa-guide exciters. The microwave is coupled to the discharge by a coaxial cable through a cavity that surrounds the quartz tube (8 mm external diameter, 6 mm internal diameter and 50 cm length). It is powered by a microwave generator

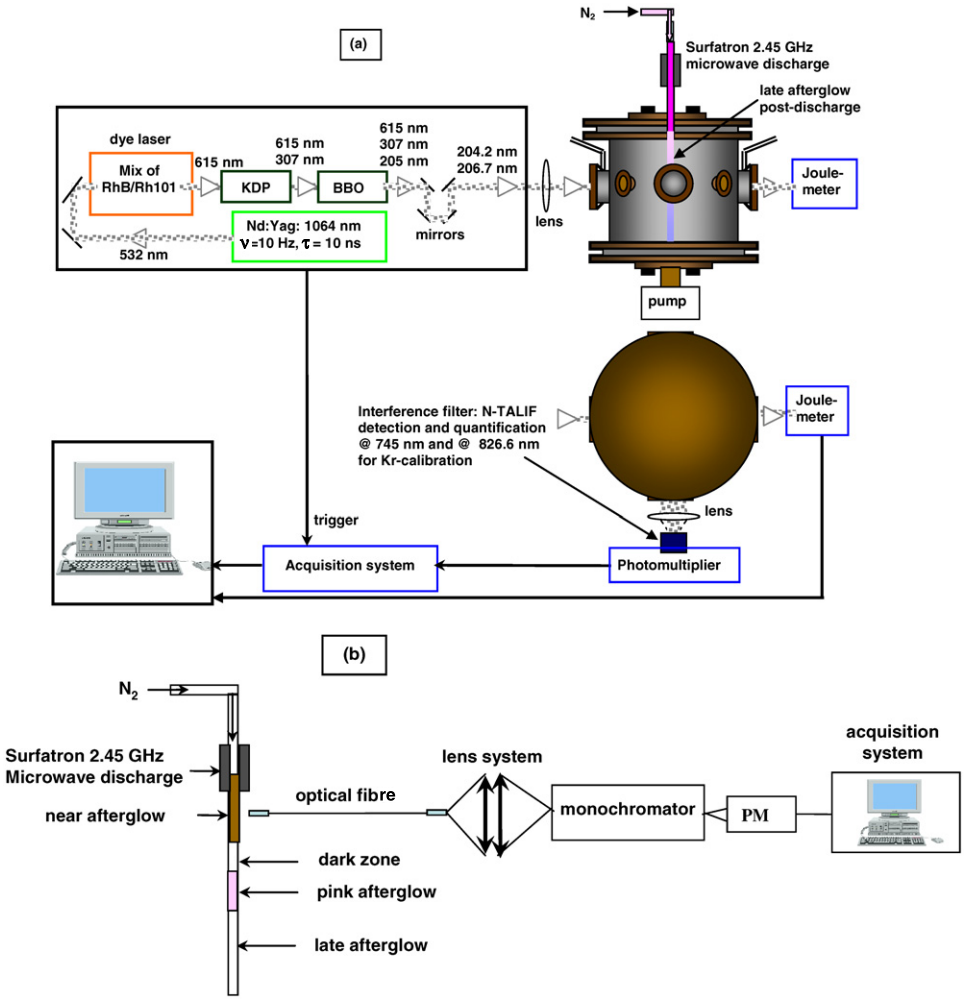

Figure 2. Experimental setup (*a*) for the TALIF spectroscopy and (*b*) scheme of microwave post-discharge with the apparatus of the OES.

(SAIREM) with a maximum power output of 300 W. The maximum reflected power is less than 2 W. An igniter coil is used to initiate the plasma in the quartz tube. The tube is connected to the reactor chamber which is a cylinder of 20 cm diameter. The microwave plasma is cooled by an air gas flow. The chamber is initially pumped down by a turbo-molecular pump to less than 10^{-4} mbar before allowing the N_2 gas flow (high purity 99.9998%). The post-discharge is flowing vertically at the centre of the vacuum chamber. The flow rate is controlled and regulated from 0 to 500 sccm (standard $cm^3\ min^{-1}$) by an MKS flow meter (type 1179B). The N_2 gas pressure measured inside the post-discharge reactor by means of a Baratron gauge (MKS 722A) is varied between 1 and 45 Torr.

The behaviour of the microwave discharge source in flowing N_2 post-discharge is investigated by OES for various parameters including microwave discharge power, N_2 gas flow rate, gas pressure and mean residence time. The analysis is performed through an optical fibre which is connected to a Jobin-Yvon HR 1000 spectrometer with a grating of $1800\ g\ mm^{-1}$ leading to a maximum resolution of 0.02 nm (figure 2(*b*)). The light is collected by a Hamamatsu photomultiplier (R636-10) connected to a chart recorder.

4. Results and discussion

4.1. Characterization of the post-discharge by OES

As shown in figure 2(*b*), flowing nitrogen microwave post-discharge can be divided into three regions: (i) the near afterglow situated close to the surfatron gap, (ii) the short-lived afterglow usually called the pink afterglow and (iii) the late afterglow named the Lewis–Rayleigh afterglow. The appearance and the dimension of each region depend mainly on the gas pressure, the flow rate, the gas temperature and the geometry of the discharge tube. In order to characterize the behaviour of each region, a systematic study by OES has been carried out along the post-discharge. Figure 3 shows the optical emission spectrum recorded between 355 and 405 nm at a resolution of 0.078 nm. The measurements are performed with a pure N_2 gas flow of 20 sccm and a gas pressure of 1 Torr. The microwave discharge power is 100 W. The optical fibre is placed perpendicularly to the quartz tube at 0.5 cm downstream from the surfatron launching gap. The dominant emission bands belong to the $\Delta v = v' - v'' = -2$ and $\Delta v = -3$ sequences of the N_2 ($C\,^3\Pi_u$, $v' \rightarrow B\,^3\Pi_g$, v'') second positive system as well as the first negative system of $N_2^+(B\,^2\Sigma_u, v' \rightarrow X\,^2\Sigma_g, v'')$ with $\Delta v = 0$ and $\Delta v = 1$.

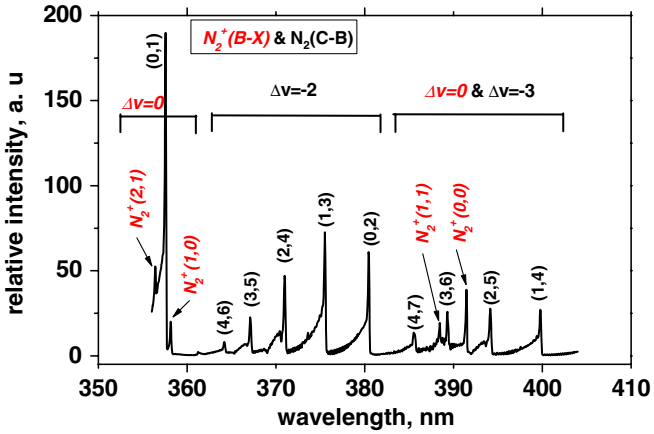

Figure 3. Emission spectrum between 355 and 405 nm recorded in N_2 flowing microwave post-discharge at 0.5 cm downstream from the surfatron launching gap. N_2 gas flow rate = 20 sccm, gas pressure = 1 Torr, microwave discharge power = 100 W, resolution = 0.078 nm.

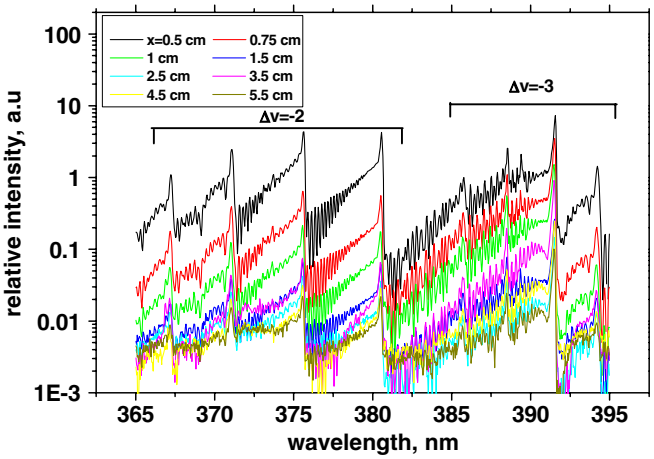

Figure 4. N_2 ($C\,^3\Pi_u \rightarrow B\,^3\Pi_g$) emission spectra between 365 and 395 nm recorded along the N_2 flowing microwave post-discharge from 0.5 to 5.5 cm downstream from the surfatron launching gap of microwave discharge. OES measurements are performed for flow rate = 200 sccm, gas pressure = 16 Torr, discharge power = 100 W, resolution = 0.078 nm.

In order to identify and to characterize the near, the pink and the late afterglow regions, series of OES measurements are obtained for different positions along the post-discharge. The optical fibre is translated perpendicularly to the quartz tube between 0.5 and 5.5 cm downstream from the surfatron launching gap. Figure 4 shows the optical emission spectrum obtained in the 365–395 nm spectral range in pure N_2 for a flow rate of 200 sccm, a gas pressure of 16 Torr and a microwave discharge power of 100 W. The emission intensities of N_2 and N_2^+ bands show strong variations and their axial profiles along the post-discharge are displayed in figure 5. Those variations can be expressed as a function of time supposing that the gas flow is laminar. The residence time t(s) is determined for each position x(cm) by $t = x/\mathrm{V}$, where V(cm s^{-1}) is the mean gas velocity given by $\mathrm{V} = (Q/\pi r^2)(760/p_{N_2})(T_g/273)(1/60)$, where Q (sccm) is the gas flow rate, r (cm) is the radius of the discharge tube, p_{N_2} (Torr) is the N_2 gas pressure and T_g (K) is the N_2 gas temperature.

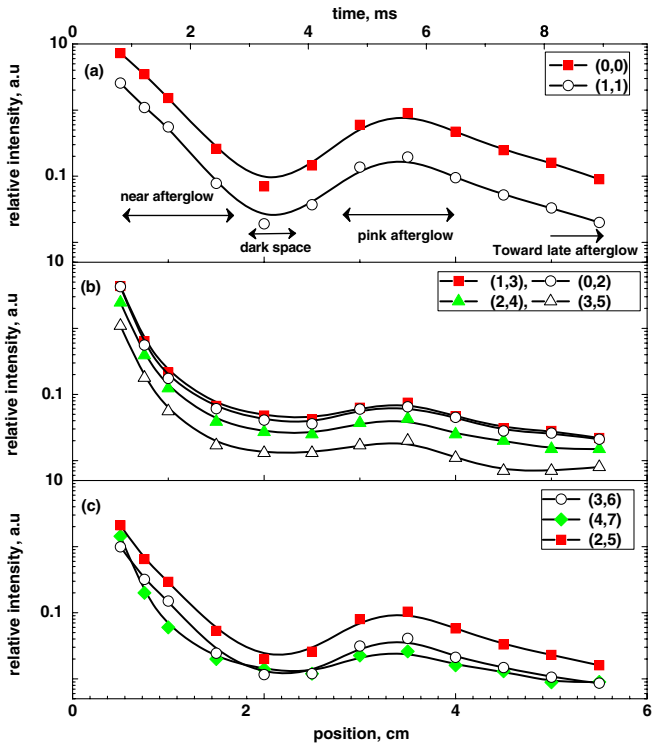

Figure 5. Axial and temporal profiles of (a) N_2^+ ($B\,^2\Sigma_u, \rightarrow X\,^2\Sigma_g$, $\Delta v = 0$), (b) N_2 ($C\,^3\Pi_u \rightarrow B\,^3\Pi_g$, $\Delta v = -2$) and (c) N_2 ($C\,^3\Pi_u \rightarrow B\,^3\Pi_g$, $\Delta v = -3$), along the N_2 flowing microwave post-discharge (near, pink and late afterglow). See figure 4 for experimental conditions.

Figure 5 allows the identification of the near, pink and late afterglow regions. The near afterglow corresponds to the region where a fast decrease of all emissions is observed. A minimum of intensity, defining the dark space, is observed at a distance of around 2 cm in our experimental conditions (200 sccm and 16 Torr). Assuming a temperature of 300 K, it corresponds to a residence time of 3.25 ms. The pink afterglow region is characterized by a significant increase in the emissions relative to the dark region. Strong emissions from the first negative system, particularly the $\Delta v = 0$ sequence, and from the second positive system $\Delta v = -2$ and $\Delta v = -3$ sequences are identified. The late afterglow corresponds to the following decrease in the intensities of the N_2^+ ($B\,^2\Sigma_u$, $v' = 0 \rightarrow X\,^2\Sigma_g$, $v'' = 0$) as well as N_2 ($C\,^3\Pi_u \rightarrow B\,^3\Pi_g$). It is observed up to a large distance downstream from the surfatron launching gap (5.5 cm, i.e. 8.9 ms in the present experimental conditions).

In order to determine the gas temperature, we focus our attention on the investigation of the strong vibrational bands of N_2 ($C\,^3\Pi_u \rightarrow B\,^3\Pi_g$) corresponding to $\Delta v = -2$: $(0-2)$, $(1-3)$, $(2-4)$ and $(3-5)$ between 365 and 382 nm (figure 6). The OES measurements are performed at 100 W and the optical fibre is moved between 0.5 and 3.5 cm downstream from the surfatron launching gap. In order to improve the signal-to-noise ratio, new conditions are used: N_2 flow rate of 20 sccm, the gas pressure is settled at 1 Torr corresponding to a residence time between 0.5 and 3.5 ms.

The rotational temperature T_r of the N_2 molecule is determined by comparing the measured and the calculated

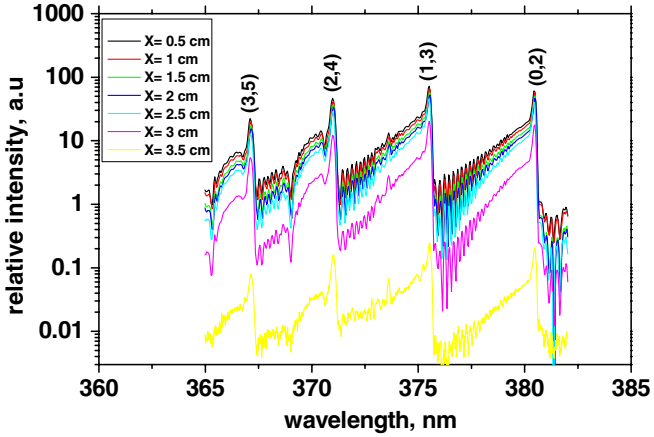

Figure 6. Measured emission N_2 ($C^3\Pi_u \rightarrow B^3\Pi_g$, $\Delta v = -2$) spectra between 365 and 382 nm used to determine the axial and temporal profile of gas temperature. N_2 gas flow rate = 20 sccm, gas pressure = 1 Torr, discharge power = 100 W, resolution = 0.078 nm.

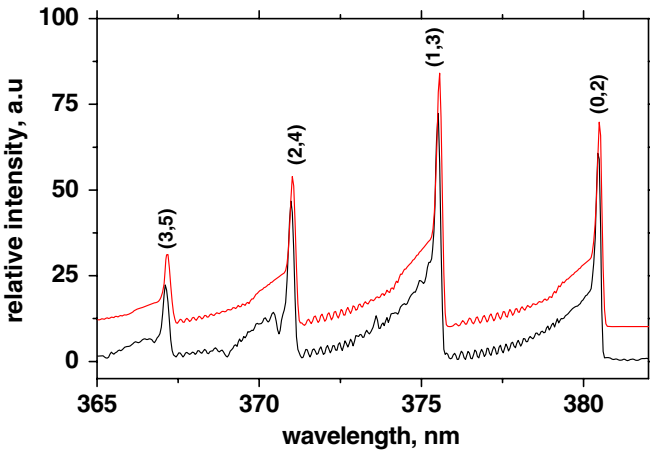

Figure 7. Examples of experimental (lower trace) and calculated (upper trace shifted upward by 10 a.u. for clarity) rovibrational bands of N_2 ($C^3\Pi_u \rightarrow B^3\Pi_g$, $\Delta v = -2$) sequence for a distance of 0.5 cm. See figure 6 for the experimental conditions.

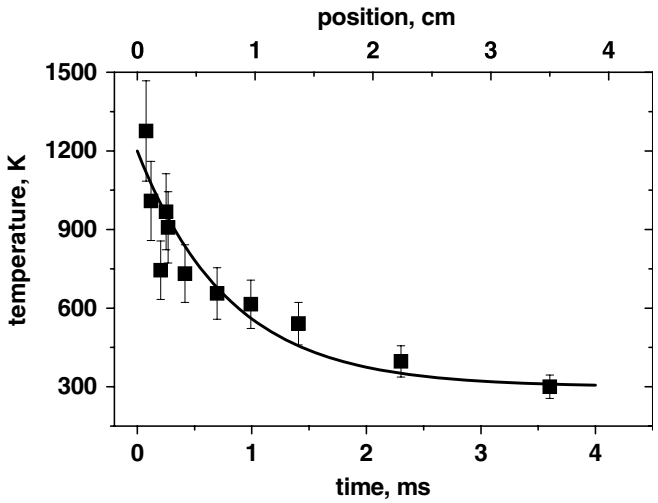

Figure 8. Axial and temporal profiles of the measured gas temperature (square) and an exponential fit (full line): $T = 300$ $(1 + 3\exp(-t/0.8))$. See figure 6 for the experimental conditions.

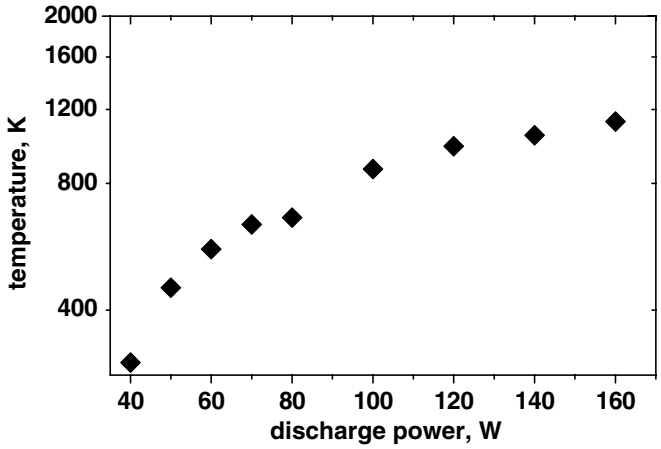

Figure 9. Measured rotational temperature as a function of the microwave discharge power. OES measurements were performed in near afterglow, at 0.5 cm downstream from the surfatron. N_2 gas flow rate = 100 sccm, gas pressure = 4 Torr.

spectra. Because of their strong intensities, the vibrational bands of N_2 ($C^3\Pi_u \rightarrow B^3\Pi_g$, $\Delta v = -2$) are most suitable to fit band contours (P, Q and R branches). The rotational temperature is fitted by a least square method considering a Boltzmann population. We assume that the rotational temperature is equivalent to the gas temperature since in the microwave discharge and at the beginning of the near afterglow region, the excited species are produced mainly by the direct electron excitation from the ground state [28]. A typical comparison between the experimental spectra and its associated synthetic spectra is presented in figure 7. As can be seen, good agreement is obtained for a temperature of 745 K at 0.5 cm. Figure 8 represents the evolution of the determined temperature along the post-discharge as a function of the residence time. The rotational temperature drops to reach a minimum around 300 K at the end of the near afterglow. This behaviour can be explained by a decrease of the electron density and the gas thermalization along the discharge tube.

The temperature of the gas also depends on the discharge power as presented in figure 9 for a flow rate of 100 sccm and a gas pressure of 4 Torr at 0.5 cm downstream from the surfatron launching gap. The microwave discharge power is varied from 40 to 160 W. For lower powers, vibrational bands $(0-2)$, $(1-3)$, $(2-4)$ and $(3-5)$ are not sufficiently intense to be reliably analysed. We clearly observe that the temperature increases from ambient temperature up to a plateau as the power increases. This can be explained by an excess energy transferred from the electrons to the neutrals leading to an increase in discharge length as the power increases. A similar behaviour has been observed by Levaton *et al* [29] in flowing nitrogen microwave discharge and by Rousseau *et al* [30] in a microwave discharge operated in argon.

The N_2 ($B^3\Pi_g$, $v' \rightarrow A^3\Sigma_u^+$, v'') first positive system is investigated between 560 and 700 nm. Different N_2 gas pressures are used in order to observe the variations of the emission of the excited species. Figure 10 reports the observed emissions corresponding to (a) the $\Delta v = 4$ sequence between

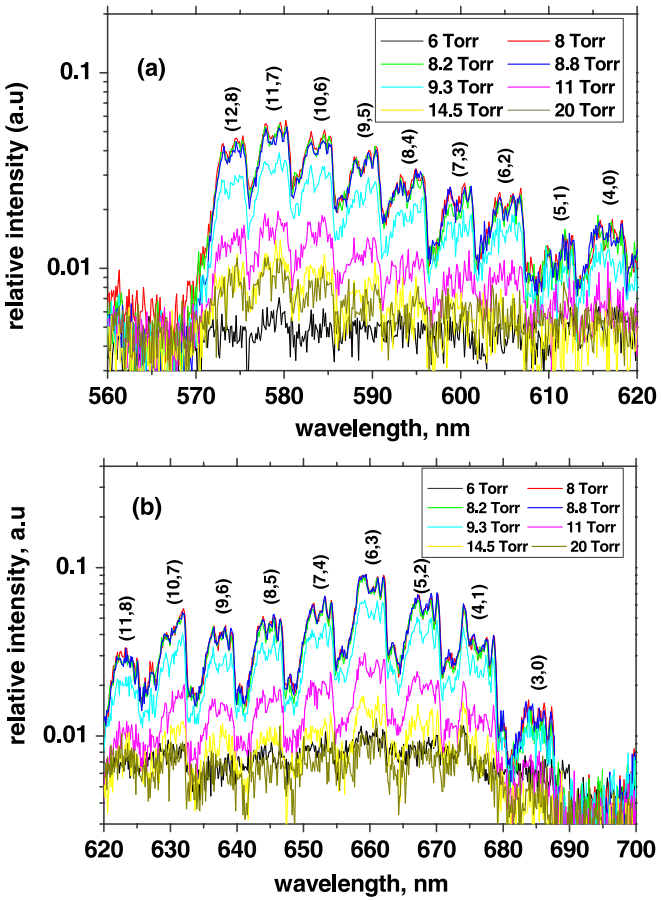

Figure 10. Measured emission spectra of N_2 ($B\,^3\Pi_g$, v'–$A\,^3\Sigma_u^+$, v''), (*a*) for $\Delta v = 4$ sequence in the 560–620 nm range and (*b*) for $\Delta v = 3$ sequence in the 620–700 nm range; recorded in N_2 flowing microwave post-discharge at 5.5 cm downstream from the surfatron launching gap. N_2 gas flow rate = 200 sccm, discharge power = 100 W, resolution = 0.5 nm.

560 and 620 nm and (*b*) the $\Delta v = 3$ sequence ranging from 620 to 700 nm. OES measurements are performed at 5.5 cm downstream from the surfatron launching gap for a 100 W microwave discharge power. The N_2 gas flow rate is 200 sccm and the pressure ranges from 6 to 20 Torr. The pressure has a strong effect on the variation of the first positive system intensity. The observed intensity is low at 6 Torr and is a maximum at around 8.8 Torr because we sound, respectively, the dark space (residence time of 3.3 ms) and the pink afterglow zone (residence time = 4.9 ms). Then the intensity slowly decreases when the pressure increases ($p_{N2} > 9.3$ Torr) indicating the presence of the late afterglow (residence time >5.5 ms) (see figure 5).

Kinetic studies of N_2^+ ($B\,^2\Sigma_u$) and N_2 ($C\,^3\Pi_u$) species along the afterglow were investigated in [31–37]. In plasma discharge and in very near afterglow, the formation of these species is attributed mainly to direct electron impacts with thresholds at about 18.5 eV for N_2^+ ($B\,^2\Sigma_u$) and about 11.1 eV for N_2 ($C\,^3\Pi_u$). Then, the density and the energy of the electrons decrease leading to the minimum emission observed in the region called the dark space (figures 5 and 10). Further in the post-discharge, we observe a re-increase of the emission (figures 5 and 10) called the pink afterglow. This behaviour cannot be explained only by direct electron impact and a sequence of elementary reactions is involved in the formation of N_2^+ ($B\,^2\Sigma_u$) and N_2 ($C\,^3\Pi_u$) species. The near-resonant V–V energy exchanges create highly vibrationally excited states of $N_2(X, v \geqslant 38)$ [31–35]. Collisions between those excited states and atomic nitrogen produce metastable N_2 ($A\,^3\Sigma_u^+$) and $N_2(a'\,^1\Sigma_u^-)$ (reactions (R_1) and (R_2), respectively) [31–35]. Furthermore, reactions between all excited species lead to N_2^+ (X)) by reaction (R_3) and (R_4) [31–35] and N_2 ($C\,^3\Pi_u$)) by reaction (R_5), (R_6) and (R_7) [35–37]. Finally, collisions between N_2^+(X) and N_2 (X,$v \geqslant 12$) through reaction (R_8) end in the formation of N_2^+ ($B\,^2\Sigma_u^+$)) [31–34, 36, 37].

$$N_2(X, v \geqslant 39) + N(^4S) \rightarrow N_2(A\,^3\Sigma_u^+) + N(^2D) \quad (R_1)$$

$$N_2(X, v \geqslant 38) + N(^4S) \rightarrow N_2(a'\,^1\Sigma_u^-) + N(^4S) \quad (R_2)$$

$$N_2(A\,^3\Sigma_u^+) + N_2(a'\,^1\Sigma_u^-) \rightarrow N_2(X\,^1\Sigma_g^+, v = 0) + N_2^+(X) + e^- \quad (R_3)$$

$$N_2(a'\,^1\Sigma_u^-) + N_2(a'\,^1\Sigma_u^-) \rightarrow N_2(X^1\Sigma_g^+, v = 0) + N_2^+(X) + e^- \quad (R_4)$$

$$N_2(A\,^3\Sigma_u^+) + N_2(A\,^3\Sigma_u^+) \rightarrow N_2\left(C\,^3\Pi_u\right) + N_2(X^1\Sigma_g^+) \quad (R_5)$$

$$N_2(X, v > 24) + N_2(X\,^1\Sigma_g^+, v > 24) \rightarrow N_2\left(C\,^3\Pi_u\right) + N_2(X) \quad (R_6)$$

$$N_2(A\,^3\Sigma_u^+) + N_2(X\,^1\Sigma_g^+, v > 19) \rightarrow N_2\left(C\,^3\Pi_u\right) + N_2(X\,^1\Sigma_g^+) \quad (R_7)$$

$$N_2^+(X) + N_2(X, v \geqslant 12) \rightarrow N_2^+(B\,^2\Sigma_u^+) + N_2(X). \quad (R_8)$$

N_2 ($B\,^3\Pi_g$) is produced by a three-body recombination between two N (^{4}S) atoms (reaction (R_9)) and as observed in figure 10, this is followed by an efficient spontaneous decay producing the first positive system (reaction (R_{10})).

$$N(^4S) + N(^4S) + N_2 \rightarrow N_2\left(B^3\Pi_g\right) + N_2 \quad (R_9)$$

$$N_2\left(B^3\Pi_g\right) \rightarrow N_2(A^3\Sigma_u^+) + h\nu. \quad (R_{10})$$

Finally, we observe the decline of the emission of all excited species in the region called the late afterglow.

4.2. TALIF measurements of absolute ground-state N (^{4}S) density

Linearity of TALIF measurements requires a two-photon mechanism. Figure 11 shows the dependence of the integrated fluorescence signals of (*a*) N ($2p^3\ ^4S_{3/2}$) and (*b*) Kr ($4p^6\ ^1S_0$) as a function of the UV energy. For UV energy below 190 μJ in the case of Kr and 150 μJ for N atoms, the slope of the linear fit of the log–log plot is 2.2 ± 0.1. Therefore, in order to determine the absolute nitrogen atom density all measurements for N (^{4}S)-TALIF are performed around 120 μJ calibrated by Kr ($4p^6\ ^1S_0$) TALIF at 76 μJ.

A TALIF study is carried out to determine the absolute ground-state N (^{4}S) atom density at 25 cm downstream from the surfatron launching gap. Figure 12 shows that the absolute N (^{4}S) density depends on the N_2 gas pressure as well as on the flow rate (i.e. on the residence time). The

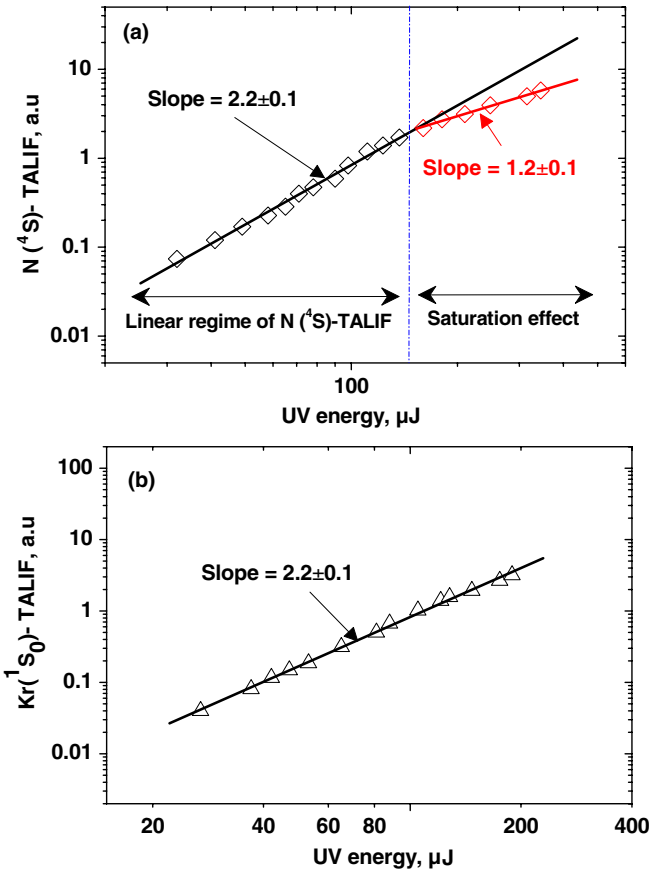

Figure 11. Log–log plot of fluorescence signals versus UV laser energy for (*a*) N ($2p^3\ ^4S_{3/2}$) in pure N_2 and (*b*) Kr ($4p^6\ ^1S_0$) in 2%Kr/N_2 mixture.

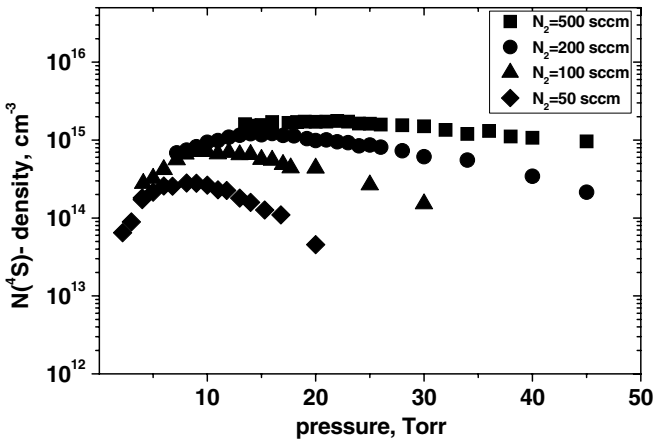

Figure 12. Absolute N ($2P^3\ ^4S_{3/2}$)-atom densities in pure N_2 measured by TALIF spectroscopy as a function of the gas pressure. All measurements of N ($2p^3\ ^4S_{3/2}$) TALIF have been performed at 25 cm downstream from the surfatron launching gap for 100 W of microwave power.

measurements are performed at a microwave power of 100 W. At a given flow rate, N (^{4}S) density increases with increasing pressure up to a maximum. When the flow rate increases, the maximum is shifted to higher pressure. A maximum value of 2.2×10^{15} cm^{-3} is obtained at 22 Torr for 500 sccm. This result is in good agreement with the value of 3×10^{15} cm^{-3}

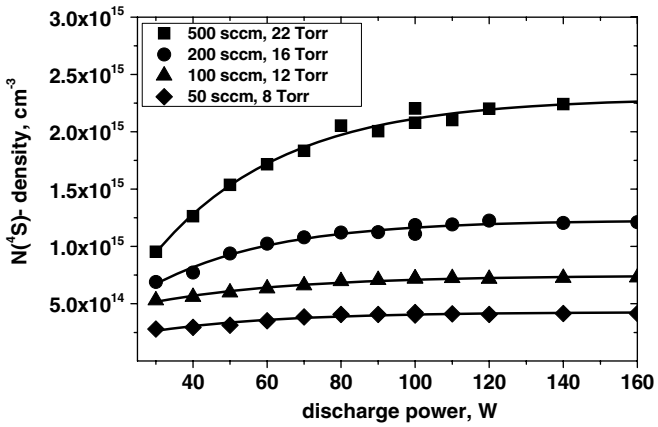

Figure 13. Absolute N ($2P^3\ ^4S_{3/2}$)-atom densities in pure N_2 measured by TALIF spectroscopy as a function of the discharge power for different values of N_2 flow rate and pressure.

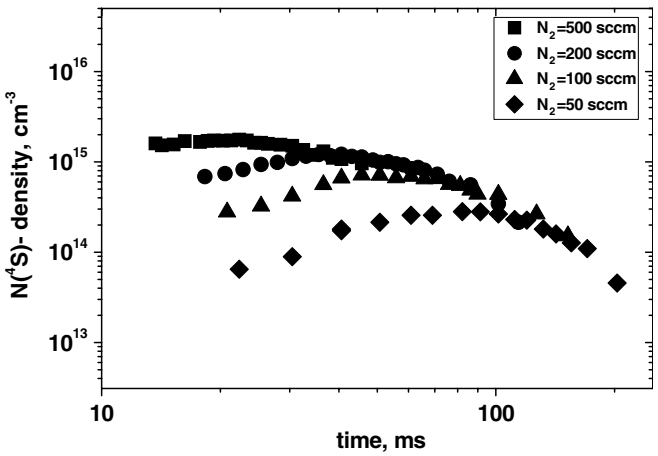

Figure 14. Absolute N ($2P^3\ ^4S_{3/2}$)-atom densities in pure N_2 measured by TALIF spectroscopy as a function of the residence time. See figure 12 for experimental conditions.

obtained by Mazouffre *et al* [26]. We have studied the effect on the maximum of N (^{4}S) density of the microwave power injected in the discharge. Figure 13 shows that it increases up to a plateau at about 100 W.

The variation of the N (^{4}S) density is represented versus the residence time in figure 14. After the maximum, the density decays with the residence time independently from the experimental conditions. According to the literature, the production of N (^{4}S) atoms in afterglow can be attributed mainly to the collisions between two N_2 ($X\ ^1\Sigma_g^+$) molecules in high vibrational levels ($10 \leqslant v \leqslant 25$) through reaction ($R_{11}$) [31, 35].

$$N_2(X\,^1\Sigma_g^+, 10 < v < 25) + N_2(X\,^1\Sigma_g^+, 10 < v < 25) \rightarrow N(^4S) + N(^4S) + N_2(X^1\Sigma_g^+, v = 0) \quad (R_{11})$$

$$N(^4S) + N(^4S) + N_2(X\,^1\Sigma_g^+) \rightarrow N_2\left(B\,^3\Pi_g, v'\right) + N_2(X\,^1\Sigma_g^+) \quad (R_{12})$$

$$N(^4S) + \text{wall} \rightarrow 1/2N_2(X\,^3\Sigma_g^+, v = 0). \quad (R_{13})$$

Metastable species N_2 ($A\,^3\Sigma_u^+$) and N (^{2}P) can also play a significant role in the chemistry in the late afterglow through [31–35]:

$$N(^2P) + N_2(X\,^1\Sigma_g^+, v \geqslant 10) \rightarrow N(^4S) + N_2(A\,^3\Sigma_u^+), \quad (R_{14})$$

$$N(^4S) + N_2(A\,^3\Sigma_u^+) \rightarrow N(^2P) + N_2(X\,^1\Sigma_g^+, 6 \leqslant v \leqslant 9). \quad (R_{15})$$

However, this cycle does not lead to a net destruction of N(^{4}S) [31–33]. Consequently, the latter is due to three-body reaction (R_{12}) and recombination on the wall (R_{13}) to form N_2 ($X\,^3\Sigma_g^+$). Then

$$\frac{d[N(^4S)]}{dt} = -k_{12}[N_2][N(^4S)]^2 - \frac{1}{\tau}[N(^4S)], \quad (3)$$

where k_{12} rate coefficient is $8.27 \times 10^{-34} \exp(500/T_g(K))\,cm^6\,s^{-1}$ [38] and τ is the characteristic time for (R_{13}): $\tau = \tau_D + \tau_{Wall}$

The characteristic diffusion time τ_D is given by

$$\tau_D = \frac{[N_2]\Lambda^2}{D_0}\left(\frac{T_g}{300}\right)^{-3/2}, \quad (4)$$

where $[N_2]$ is the total nitrogen density at a given gas pressure, $\Lambda \approx (R/2.405)$ is the characteristic diffusion length, with $R = 0.3$ cm the tube radius, $D_0 = 7.9 \times 10^{18}\,cm^{-1}\,s^{-1}$ is the reduced diffusion coefficient taken from [39] and T_g is the gas temperature. Considering that the gas pressure is less than 45 Torr and $T_g = 300$ K, τ_D does not exceed 2.8 ms. This has to be compared with the characteristic time of wall recombination τ_{Wall} given by

$$\tau_{Wall} = 2R/\gamma V_M, \quad (5)$$

where γ is the wall recombination probability and V_M is the mean thermal velocity. The corresponding characteristic decay time τ_{Wall} of N (^{4}S) atoms is between 64 ms and ~4 s depending on the value of γ which varies in the literature from 2×10^{-4} to 3.2×10^{-6} [40, 41]. Therefore, the diffusion time can be neglected and the characteristic time for (R_{13}), $\tau = \tau_{Wall}$.

The density of N (^{4}S) as a function of time can be obtained from (3) and is given by

$$[N(^4S)](t) = \left\{\left(\frac{1}{[N_0]} + \tau\, k_{12}[N_2]\right)e^{t/\tau} - \tau\, k_{12}[N_2]\right\}^{-1}, \quad (6)$$

where $[N_0]$ is the initial N (^{4}S) at $t = 0$ extrapolated from figure 13: $[N_0] = 3 \times 10^{15}\,cm^{-3}$. Equation (6) has been used to model the experimental data setting γ as a free parameter (figure 15). A γ value of $(2.1 \pm 0.3) \times 10^{-4}$ is obtained. This is in agreement with the one measured by Young and Boudart [40] and typically used to describe the spatial structure of post-discharges [35]. The value of 3.2×10^{-6} determined by Yamashita [41] can be definitively ruled out since such a low value would correspond to a characteristic decay time of ≈4s incompatible with the residence time of N (^{4}S) in our tube.

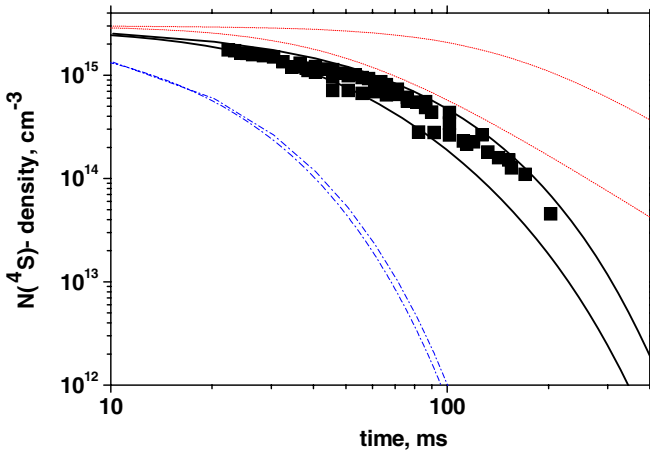

Figure 15. N (^{4}S)-atom density as a function of the residence time: comparison between measurements (square) and modelling for different values of γ (dotted line: 3.2×10^{-6}; full line: 2.1×10^{-4}; dashed–dotted line: 1×10^{-3}). In each case, the upper line is for a flow rate of 50 sccm and the lower line is for 500 sccm.

5. Conclusion

We have reported the characterization of the microwave flowing post-discharge sustained at 2.45 GHz in pure nitrogen by optical emission spectroscopy and the measurement of the absolute nitrogen atom densities using TALIF spectroscopy in the experimental conditions of the gas pressure range 1–45 Torr, nitrogen gas flow rate between 20 and 500 sccm and microwave discharge power from 30 to 160 W.

OES has been performed in order to determine the axial and temporal profiles of N_2^+ ($B\,^2\Sigma_u$, $v' \rightarrow X\,^2\Sigma_g$, v'') and N_2 ($C\,^3\Pi_u \rightarrow B\,^3\Pi_g$, $\Delta v = -2$, $\Delta v = -3$) emissions along the post-discharge. The observed evolution of the radiative species allows defining the near, pink and late afterglow. The highest rotational temperature (1200 K) is reached in the near afterglow for a discharge power of 160 W. The temperature decreases down to room temperature in the late afterglow.

We have measured the absolute density of ground-state nitrogen atoms in the late afterglow by TALIF spectroscopy diagnostic using krypton as a reference gas. The N-atom densities have been studied as a function of N_2 gas flow rate, gas pressure and microwave discharge power. The kinetic of N-atom densities depend mainly on the residence time. The densities increase as the time increases up to a maximum, and then the atoms destruction overcomes the nitrogen atom production. The maximum of N-atom densities is around $2.2 \times 10^{15}\,cm^{-3}$ at 22 Torr for 500 sccm. The decay of N-atom density as a function of time can be modelled taking into account losses by three-body reaction in the volume and recombination on wall surface. The wall recombination probability $\gamma = (2.1 \pm 0.3) \times 10^{-4}$ is obtained for quartz.

Acknowledgments

This work takes place in the frame of the SETUP (a French acronym for Experimental and Theoretical Simulations Useful for Planetology) programme developed in our laboratory. This programme is performed under financial support from the

French Space Agency (Centre National d'Etudes Spatiales, CNES), from the Ile de France Region (SESAME grant) and the French National Programme of Planetary Sciences (PNP). The main author acknowledges the Centre National de la Recherche Scientifique (CNRS) for its post-doctoral grant.

References

[1] Ricard A, Oseguera-Pena J E, Falk L, Michel H and Gantois M 1990 Active species in microwave postdischarge for steel-surface nitriding *IEEE Trans. Plasma Sci.* **18** 940

[2] Michel H, Czerwiec T, Gantois M, Ablitzer D and Ricard A 1995 Progress in the analysis of the mechanisms of ion nitriding *Surf. Coat. Technol.* **72** 103

[3] Normand F, Marec J, Leprince Ph and Granier A 1991 Surface treatment of polypropylene by oxygen microwave discharge *Mater. Sci. Eng.* A **139** 103

[4] Guymont O, LeDuc E, Pagnon D, Pointu A M, Touzeau M, Vialle M, Mercey B and Murray H 1992 Atomic oxygen radio-frequency source and its application to the treatment of mixed valence copper oxide thin films *Plasma Sources Sci. Technol.* **1** 175

[5] Ricard A, Moisan M and Moreau S 2001 Détermination de la concentration d'oxygène atomique par titrage avec NO dans une post-décharge en flux, émanant de plasmas de Ar–O_2 et N_2–O_2, utilisée pour la stérilisation *J. Phys. D: Appl. Phys.* **34** 1203

[6] Boudam M K, Saoudi B, Moison M and Ricard A 2007 Characterization of the flowing afterglows of an N_2–O_2 reduced-pressure discharge: setting the operating conditions to achieve a dominant late afterglow and correlating the NO_β UV intensity variation with the N and O atom densities *J. Phys. D: Appl. Phys.* **40** 1694–711

[7] Moisan M, Barbeau J, Moreau S, Pelletier J, Tabrizian M and Yahia L H 2001 Low-temperature sterilization using gas plasmas: a review of the experiments and an analysis of the inactivation mechanisms *Int. J. Pharmaceut.* **226** 1

[8] Monna V, Nguyen C, Kahil M, Ricard A and Sixou M 2002 Sterilization of dental bacteria in a flowing N_2–O_2 postdischarge reactor *IEEE Trans. Plasma Sci.* **30** 1437

[9] Pintassilgo C D and Loureiro J 2006 Kinetic modelling of a N_2–CH_4 microwave discharge for a wide range of pressures for simulation of Titan's atmosphere *European Planetary Science Congress (EPSC) (Berlin, Germany)*

[10] Pintassilgo C D and Loureiro J 2008 Kinetic study of an afterglow plasma for simulation of Titan's atmosphere *19th Europhys. Conf. on the Atomic and Molecular Physics of Ionized Gases (Granada, Spain, 15–19 July)*

[11] Es-sebbar Et, Benilan Y, Arzoumanian E and Gazeau M C 2008 TALIF quantification of nitrogen atoms applied to experimental simulation of Titan's atmosphere *37th COSPAR (Montreal, Canada, 13-20 July)*

[12] Gazeau M C, Es-sebbar Et, Arzoumanian E, Perrier S and Bénilan Y 2008 SETUP Experimental and Theoretical Simulations Useful for Planetology related studies on molecular nitrogen dissociation by cold plasma *European Planetary Science Congress (Münster, Germany, 21–26 September)*

[13] Amorim J, Baravian G and Jolly J 2000 Laser-induced resonance fluorescence as a diagnostic technique in non-thermal equilibrium plasmas *J Phys. D: Appl. Phys.* **33** R51–65

[14] Sasaki K, Nakamoto M and Kadota K 2001 A measurement method of absolute hydrogen atom density in plasmas by (2 + 1)-photon laser-induced fluorescence spectroscopy *Rev. Sci. Instrum.* **72** 2298

[15] A Broc A, Benedictis S De and Dilecce G 2004 LIF investigations on NO, O and N in a supersonic N_2/O_2/NO RF plasma jet *Plasma Sources Sci. Technol.* **13** 504–14

[16] Williamson James M and Ganguly Biswa N 2000 Hydrogen dissociation in a H_2–N_2 pulsed dc glow discharge *Phys. Rev.* E **61** 5734–42

[17] Adams S F and Miller T A 1998 Two-photon absorption laser-induced fluorescence of atomic nitrogen by an alternative excitation scheme *Chem. Phys. Lett.* **295** 305–11

[18] Döbele H F, Mosbach T, Niemi K and Gathen V Schulz-von der 2005 Laser-induced fluorescence measurements of absolute atomic densities: concepts and limitations *Plasma Sources Sci. Technol.* **14** S31–41

[19] Es-sebbar Et, Gherardi N and Massines F 2007 N, O and NO concentration in N_2/O_2 and N_2/N_2O Townsend Dielectric Barrier Discharge *18th Int. Symp. on Plasma Chemistry (Kyoto, Japan, 26–31 August)*

[20] Gherardi N, Es-sebbar Et, Naudé N and Massines F 2008 Investigations of homogeneous dielectric barrier discharge in N2: LIF, TALIF and electrical measurements *61st Annual Gaseous Electronics Conf. (GEC) (Dallas, TX, USA, 13–17 October)*

[21] Niemi K, Schulz-von der Gathen V and Döbele H F 2005 Absolute atomic oxygen density measurements by two-photon absorption laser-induced fluorescence spectroscopy in an RF-excited atmospheric pressure plasma jet *Plasma Sources Sci. Technol.* **14** 375–86

[22] Kulatilaka Waruna D, Lucht Robert P, Hanna Sherif F and Katta Viswanath R 2004 Two-color, two-photon laser-induced polarization spectroscopy (LIPS) measurements of atomic hydrogen in near-adiabatic, atmospheric pressure hydrogen/air flames *Combustion Flame* **137** 523–37

[23] Grützmacher K, de la Rosa M.I, Gonzalo A.B, Steiger M, Steiger A 2003 Two-photon polarization spectroscopy applied for quantitative measurements of atomic hydrogen in atmospheric pressure flames *Appl. Phys. B: Lasers Opt.* **76** 775–85

[24] Lukas C, Spaan M, Schulz-von der Gathen V, Thmoson M, Wegst R, Döbele H F and Neiger M 2001 Dielectric barrier discharges with steep voltage rise: mapping of atomic nitrogen in single filaments measured by laser-induced fluorescence spectroscopy *Plasma Sources Sci. Technol.* **10** 445–50

[25] Boogaarts M G H, Mazouffre S, Brinkman G J, van der Heijden H W P, Vankan P, van der Mullen J J A M, Scram D C and Döbele H F 2002 Quantitative two-photon laser-induced fluorescence measurements of atomic hydrogen densities, temperatures, and velocities in an expanding thermal plasma *Rev. Sci. Instrum.* **73** 73–86

[26] Mazouffre S, Foissac C, Supiot P, Engeln R, Vankan P J W, Schram D C and Sadeghi N 2001 Density and temperature of N atoms in the afterglow of a microwave discharge measured by a two-photon laser-induced fluorescence technique *Plasma Sources Sci. Technol.* **10** 168–75

[27] Niemi K, Schulz-von der Gathen V and Döbele H F 2001 Absolute calibration of atomic density measurements by laser-induced fluorescence spectroscopy with two-photon excitation *J. Phys. D: Appl. Phys.* **34** 2330–5

[28] Drake D J, Popović S and Vušković L 2008 Characterization of a supersonic microwave discharge in Ar/H_2/Air mixtures *J. Appl. Phys.* **104** 063305

[29] Levaton J, Ricard A, Henriques J, Silva H R T and Amorim J 2006 Measurements of N(^{4}S) absolute density in a 2.45 GHz surface wave discharge by optical emission spectroscopy *J. Phys. D: Appl. Phys.* **39** 3285–93

[30] Rousseau A, Teboul E, Sande M J v d and van der Mullen J J A M 2002 Spatially resolved gas

temperature measurements by Rayleigh scattering in a microwave discharge *Plasma Sources Sci. Technol.* **11** 47-52

[31] Sá P A, Guerra V, Loureiro J and Sadeghi N 2004 Self-consistent kinetic model of the short-lived afterglow in flowing nitrogen *J. Phys. D: Appl. Phys.* **37** 221–31

[32] Guerra V, Sá P A and Loureiro J 2003 Electron and metastable kinetics in the nitrogen afterglow *Plasma Sources Sci. Technol.* **12** S8–15

[33] Loureiro J, Sá P A and Guerra V 2006 On the difficulty of N (^{4}S) atom recombination to explain the appearance of the pink afterglow in a N_2 flowing discharge *J. Phys. D: Appl. Phys.* **39** 122–5

[34] Loureiro J, Sá P A and Guerra V 2001 Role of long-lived $N_2(X\,^1\Sigma_g^+,v)$ molecules and $N_2(A\,^3\Sigma_u^+)$ and $N_2(a'\,^1\Sigma_u^-)$ states in the light emissions of an N_2 afterglow, *J. Phys. D: Appl. Phys.* **34** 1769–78

[35] Henriques J, Tatarova E, Dias F M and Ferreira C M 2008 Spatial structure of a slot-antenna excited microwave N_2–Ar plasma source *J. Appl. Phys.* **103** 103304

[36] Gómez B J, Brühl S P, Feugeas J N and Ricard A 1999 The time variations of N_2 active species in pulsed N_2-H_2 dc discharges *J. Phys. D: Appl. Phys.* **32** 1239–42

[37] Brühl S P, Russell M W, Gómez B J, Grigioni G M, Feugeas J N and Ricard A 1997 A study by emission spectroscopy of the N_2 active species in pulsed dc discharges *J. Phys. D: Appl. Phys.* **30** 2917–22

[38] Kossyi I A, Kostinsky A Yu, Matveyev A A and Silakov V P 1992 Kinetic scheme of the non-equilibrium discharge in nitrogen–oxygen mixtures *Plasma Sources Sci. Technol.* **1** 207–20

[39] Cernogora G and Sadeghi N1980 Diffusion coefficients of $N^*(^2D)$ and $N^*(^2P)$ in N_2 *Chem. Phys. Lett.* **74** 417–20

[40] Young C K and Boudart M 1991 Recombination of O, N, and H atoms on silica: kinetics and mechanism *Langmuir* **7** 2999–3005

[41] Yamashita T 1979 Rate of recombination of nitrogen atoms *J. Chem. Phys.* **70** 4248